Composite Majorana fermion wave functions in nanowires

Jelena Klinovaja and Daniel Loss

Department of Physics, University of Basel, Klingelbergstrasse 82, 4056 Basel, Switzerland

We consider Majorana fermions (MFs) in quasi-one-dimensional nanowire systems containing normal and superconducting sections where the topological phase based on Rashba spin-orbit interaction can be tuned by magnetic fields. We derive explicit analytic solutions of the MF wave function in the weak and strong spin orbit interaction regimes. We find that the wave function for one single MF is a composite object formed by superpositions of different MF wave functions which have nearly disjoint supports in momentum space. These contributions are coming from the extrema of the spectrum, one centered around zero momentum and the other around the two Fermi points. As a result, the various MF wave functions have different localization lengths in real space and interference among them leads to pronounced oscillations of the MF probability density. For a transparent normal-superconducting junction we find that in the topological phase the MF leaks out from the superconducting into the normal section of the wire and is delocalized over the entire normal section, in agreement with numerical results obtained in previous studies.

I. INTRODUCTION

Majorana fermions[1] (MFs), being their own antiparticles, have attracted much attention in recent years in condensed matter physics.[2–19] Besides being of fundamental interest, these exotic quantum particles have the potential for being used in topological quantum computing due to their non-Abelian statistics.[20–26] There are a number of systems in which to expect MFs, e.g., fractional quantum Hall systems,[27,28] topological insulators,[3,4] optical lattices,[5] *p*-wave superconductors,[12] and especially nanowires with strong Rashba spin-orbit interaction[7–9]—the system of interest in this work. There are now several claims for experimental evidence of MFs in topological insulators[29,30] and, in particular, in semiconducting nanowires of the type considered here.[31–33]

As is well known,[7–9,19] an *s*-wave superconductor brought into contact with a semiconducting nanowire with Rashba spin-orbit interaction (SOI) induces effective *p*-wave superconductivity that gives rise to MFs, one at each end of such a wire. Most studies have analyzed the corresponding model Hamiltonian by direct numerical diagonalization, which provides exact solutions of the Schrödinger equation for essentially all parameter values irrespective of their relative sizes. Less attention, however, has been given to analytical approaches which can provide additional insights into the nature of MFs. As usual, this comes with a price: closed analytic expressions are hard to come by and can be obtained only in special limits. But since these limits turn out to include realistic parameter regimes such an approach is not a mere academic exercise but worthwhile also from a physical point of view.

Motivated by this, we focus in the present work on the spinor wave function for MFs, and derive analytical expressions for various limiting cases, loosely characterized as weak and strong SOI regimes. We find that these solutions are superpositions of states that come, in general, from different extremal points of the energy dispersion, one centered around zero momentum and the others around the Fermi points. Despite having nearly disjoint support in momentum space, all such contributions must be taken into account, in general, in order to satisfy the boundary conditions imposed on the spinor wave

functions in real space. As a consequence of this composite structure of the MF wave functions, there will be more than one localization length that characterizes a single MF. We will see throughout this work that the Schrödinger equation for the systems under consideration allows, in principle, degenerate MF wave functions. However, this degeneracy gets completely removed by the boundary conditions considered here, and, consequently, there exists only one single MF wave function at a given end of the nanowire. The superposition also gives rise to interference effects that leads to pronounced oscillations of the MF probability density in real space. Quite interestingly, the relative strengths of the different localization lengths as well as of the oscillation periods can be tuned by magnetic fields.

If only a section of the wire is covered with a superconductor, a normal-superconducting (NS) junction is formed. For this case, we find that the MF becomes delocalized over the entire normal section, while still localized in the superconducting section, as noted by several groups before,[19,34–37] and most recently studied in detail in a numerical study by Chevallier *et al.*[38] Here, we will find analytical solutions for this problem, valid in the weak and strong SOI regime. Depending on the length of the normal section, the support of the MF wave function is, again, centered at zero momentum or the Fermi momenta. Also similarly as before, different localization lengths and oscillation periods of the MF in the normal section occur, again tunable by magnetic fields. This could then provide an experimental signature for MFs, e.g., in a tunneling density of states measurement, where a signal that comes from a zero-mode MF will show oscillations along the normal section.

The paper is organized as follows. In Sec. II we introduce the continuum model of a nanowire including SOI, magnetic field, and induced superconductivity. The composite structure of MF in proximity-induced superconducting wire is discussed in Sec. III for strong and weak SOI. In Sec. IV we investigate an NS junction and show how the type of MF wave function oscillates in space and depends on magnetic field. The final Sec. V contains our conclusions. Some technical details are referred to two appendixes.
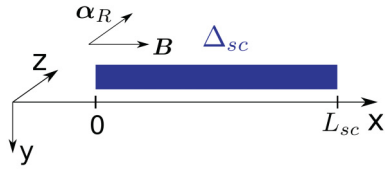
FIG. 1. (Color online) Nanowire (blue slab) of length L_{sc} in the superconducting regime with gap Δ_{sc} induced via proximity effect by a bulk s-wave superconductor (not shown). A magnetic field **B** is applied along the nanowire in x direction and perpendicularly to the Rashba SOI vector $\boldsymbol{\alpha}_R$ that points in z direction.

II. MODEL

Following earlier work,[7–9,19,38] our starting point is a semiconducting nanowire with Rashba SOI (see Fig. 1) characterized by a SOI vector $\boldsymbol{\alpha}_R$ that points perpendicularly to the nanowire axis and defines the spin quantization direction z. In addition, a magnetic field **B** is applied along the nanowire in the x direction. We imagine that the nanowire (or a section of it) is in tunnel contact with a conventional bulk s-wave superconductor which leads to proximity-induced superconductivity in the nanowire itself, characterized by the induced s-wave gap Δ_{sc} (see Fig. 1). We refer to this part of the nanowire as the superconducting section (or as the nanowire being in the superconducting regime), in contrast to the "normal" section of the nanowire that is not in contact with the superconductor and thus in the normal regime.

We describe this nanowire system by a continuum model and our goal is to find the explicit wave functions for the MFs in the entire nanowire, including the normal and superconducting section. For this, we need to introduce some basic definitions and briefly recall well-known results about the spectrum.

The Hamiltonian $H^0 = H^{\rm kin} + H^{\rm SOI} + H^Z$ for the normal regime[7,8] consists of the kinetic energy term

$$H^{\rm kin} = \sum_\sigma \int dx \ \Psi_\sigma^\dagger(x) \left[\frac{(-i\hbar\partial_x)^2}{2m} - \mu \right] \Psi_\sigma(x), \quad (1)$$

where m is the (effective) electron mass, and μ is the chemical potential, the SOI term,

$$H^{\rm SOI} = -i\alpha_R \sum_{\sigma,\sigma'} \int dx \ \Psi_\sigma^\dagger(x)(\sigma_3)_{\sigma\sigma'}\partial_x \Psi_{\sigma'}(x), \quad (2)$$

where, again, the z axis is chosen along $\boldsymbol{\alpha}_R$, and the Zeeman term corresponding to the magnetic field B along the nanowire (x axis),

$$H^Z = \Delta_Z \sum_{\sigma,\sigma'} \int dx \ \Psi_\sigma^\dagger(x)(\sigma_1)_{\sigma\sigma'}\Psi_{\sigma'}(x). \quad (3)$$

Here, $\Psi_\sigma^\dagger(x)$ is the creation operator of an electron at position x with spin $\sigma/2 = \pm 1/2$ (along the z axis), and the Pauli matrices $\sigma_{1,2,3}$ act on the spin of the electron. The Zeeman energy is given by $\Delta_Z = g\mu_B B/2$, where g is the g factor, and μ_B is the Bohr magneton. It is convenient to introduce the corresponding Hamiltonian density $\mathcal{H}^0$,

$$H^0 = \int dx \ \psi^\dagger(x)\mathcal{H}^0\psi(x),$$
$$\mathcal{H}^0 = -\hbar^2\partial_x^2/2m - \mu - i\alpha_R\sigma_3\partial_x + \Delta_Z\sigma_1, \quad (4)$$
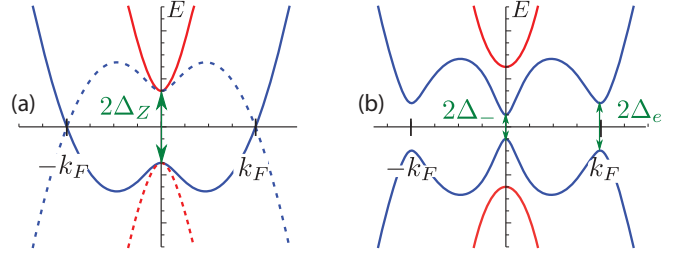

FIG. 2. (Color online) Bulk spectrum for extended electron (solid lines) and hole (dashed lines) states in the normal (a) and in the superconducting regime (b). (a) In the normal regime, a Zeeman gap $2\Delta_Z$ is opened at $k = 0$, but the full spectrum is still gapless due to the propagating modes at the Fermi points $\pm k_F$. (b) The proximity-induced superconductivity leads to the opening of a gap Δ_e at the Fermi points $\pm k_F$ and modifies the topological gap $\Delta_- = \Delta_{sc} - \Delta_Z$ at $k = 0$.

which acts on the vector $\psi = (\Psi_\uparrow, \Psi_\downarrow)$. The bulk spectrum of $\mathcal{H}^0$ [see Fig. 2(a)] consists of two branches and is given by

$$E_\pm^0(k) = \frac{\hbar^2 k^2}{2m} - \mu \pm \sqrt{(\alpha_R k)^2 + \Delta_Z^2}, \quad (5)$$

where k is a momentum along the nanowire. By opening a Zeeman gap $2\Delta_Z$, the magnetic field lifts the spin degeneracy at $k = 0$. The chemical potential μ is tuned inside this gap and set to zero. In this case, the Fermi wave vector is determined from $E_-^0(k_F) = 0$ and given by

$$k_F = \sqrt{2k_{\rm so}^2 + \sqrt{4k_{\rm so}^4 + k_Z^4}}, \quad (6)$$

where $k_{\rm so} = m\alpha_R/\hbar^2$ and $k_Z = \sqrt{2\Delta_Z m}/\hbar$.

The nanowire in the superconducting regime is described by the Hamiltonian $H^0 + H^{sc}$, where the s-wave BCS Hamiltonian H^{sc} couples states with opposite momenta and spins,[7,8]

$$H^{sc} = \frac{1}{2} \sum_{\sigma,\sigma'} \int dx \ \Delta_{sc}(\Psi_\sigma(i\sigma_2)_{\sigma\sigma'}\Psi_{\sigma'} + {\rm H.c.}). \quad (7)$$

The proximity-induced superconductivity gap Δ_{sc} is chosen to be real (thereby assuming that we can neglect the flux induced by the B field, which is the case, e.g., for InSb nanowires[31]). The spectrum of $H^0 + H^{sc}$ [see Fig. 2(b)] is then found to be

$$E_\pm^2(k) = \left(\frac{\hbar^2 k^2}{2m} \right)^2 + (\alpha_R k)^2 + \Delta_Z^2 + \Delta_{sc}^2$$
$$\pm 2\sqrt{\Delta_Z^2\Delta_{sc}^2 + \left(\frac{\hbar^2 k^2}{2m} \right)^2 [\Delta_Z^2 + (\alpha_R k)^2]}. \quad (8)$$

The "topological" gap at $k = 0$ is given by $\Delta_- = \Delta_{sc} - \Delta_Z$, and the closing of this gap marks the transition between non-topological ($\Delta_- > 0$) and topological ($\Delta_- < 0$) phases.[5,7,8] In contrast, the gap at k_F, $\Delta_e \equiv 2|E_-(k_F)|$, is always nonzero [see Fig. 2(b)].

III. MAJORANA FERMIONS IN THE SUPERCONDUCTING SECTION

In this section we consider first the simpler case where the superconducting section extends over the entire nanowire
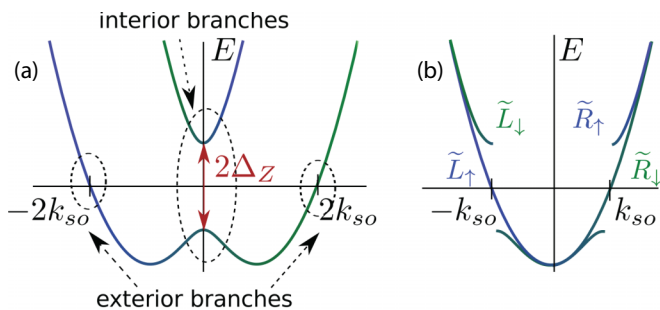
FIG. 3. (Color online) (a) Band structure of a nanowire with strong SOI and in a uniform magnetic field B in the laboratory frame (see also Fig. 2) for the normal section. States around $k = 0$ belong to the interior branches and states around $k = k_F = 2k_{so}$ belong to the exterior branches. (b) The same band structure in the rotating frame. The rotating magnetic field $\widetilde{\mathbf{B}}(x)$ given by Eq. (12) couples $\widetilde{R}_\uparrow$ and $\widetilde{L}_\downarrow$ that leads to the opening of the Zeeman gap $2\Delta_Z$ but does not affect $\widetilde{L}_\uparrow$ and $\widetilde{R}_\downarrow$.

from $x = 0$ to $x = L_{sc}$; see Fig. 1. In the topological phase there is one MF bound state at each end of the nanowire.[7,8] In the physically interesting regime, these two MFs should be independent and have negligible spatial overlap. This justifies the consideration of a semi-infinite nanowire. In this work we focus on the MF at the left end, $x = 0$.

We will consider two limiting regimes, namely strong ($k_F \simeq 2k_{so}$) and weak ($k_F \simeq k_Z$) SOI. In both regimes, the Hamiltonian can be linearized near the Fermi points and solved analytically. We show that the MF wave function has support in k space from the exterior ($k \simeq \pm k_F$) and the interior ($k \simeq 0$) branches of the spectrum; see Fig. 3(a). If the system is in some intermediate regime of moderate SOI, the support of the MF wave function extends over all momenta from $-k_F$ to k_F, and this case cannot be treated analytically in the linearization approximation considered here.

A. Regime of strong SOI and rotating frame

The regime of strong SOI is defined by the condition that the SOI energy at the Fermi level is larger than the Zeeman splitting, $\Delta_Z \ll m\alpha_R^2/\hbar^2$ (or $k_F \approx 2k_{so}$), and larger than the proximity gap, $\Delta_{sc} \ll m\alpha_R^2/\hbar^2$. This allows us to treat the magnetic field and the proximity-induced superconductivity as small perturbations.

The spectrum obtained in Eq. (5) consists of two parabolas shifted by the SOI momentum $k_{so} = m\alpha_R/\hbar^2$ and with a Zeeman gap opened at $k = 0$ [see Fig. 3(a)]. In the strong SOI regime it is more convenient to work in the rotating frame; see Fig. 3(b). For this we follow Ref. 39 and make use of the following spin-dependent gauge transformation

$$\Psi_\sigma(x) = e^{-i\sigma k_{so}x}\widetilde{\Psi}_\sigma(x), \tag{9}$$

where the tilde refers to the rotating frame. The H^{SOI} term is effectively eliminated ($\widetilde{H}^{\mathrm{SOI}} = 0$) and the spectrum corresponding to $\widetilde{H}^{\mathrm{kin}}$ consists of two parabolas centered at $k = 0$, one for spin up and one for spin down. Around the Fermi points, $\pm k_{so}$, the spectrum can be linearized and electron operators $\widetilde{\Psi}_\sigma$ are expressed in terms of slowly varying

right ($\widetilde{R}_\sigma$) and left ($\widetilde{L}_\sigma$) movers,

$$\widetilde{\Psi}_\sigma(x) = \widetilde{R}_\sigma(x)e^{ik_{so}x} + \widetilde{L}_\sigma(x)e^{-ik_{so}x}. \tag{10}$$

The kinetic-energy term in the linearized model is

$$\widetilde{H}^{\mathrm{kin}} = -i\hbar\upsilon_F \int dx\, [\widetilde{R}_\sigma^\dagger(x)\partial_x\widetilde{R}_\sigma(x) - \widetilde{L}_\sigma^\dagger(x)\partial_x\widetilde{L}_\sigma(x)] \tag{11}$$

with Fermi velocity $\upsilon_F = \alpha_R/\hbar$. Here, we dropped all fast oscillating terms, which is justified as long as $\xi \gg 2\pi/k_{so}$, where ξ is a localization length of $\widetilde{R}_\sigma$ and $\widetilde{L}_\sigma$ (see below).

In the rotating frame the B field becomes helical, rotating in the plane perpendicular to the SOI vector $\boldsymbol{\alpha}_R$,

$$\widetilde{\mathbf{B}}(x) = B[\hat{x}\cos(2k_{so}x) - \hat{y}\sin(2k_{so}x)]. \tag{12}$$

Here, $\hat{x}$ and $\hat{y}$ are unit vectors in x and y directions, respectively (see Fig. 1). This leads to the Zeeman Hamiltonian of the form

$$\widetilde{H}^Z = \Delta_Z \int dx\, \widetilde{\Psi}_\sigma^\dagger(x)e^{2i\sigma k_{so}x}\widetilde{\Psi}_{-\sigma}(x),$$

$$\simeq \Delta_Z \int dx\, [\widetilde{R}_\uparrow^\dagger(x)\widetilde{L}_\downarrow(x) + \widetilde{L}_\downarrow^\dagger(x)\widetilde{R}_\uparrow(x)], \tag{13}$$

where in the second line we used the linearization approximation and, again, dropped all fast oscillating terms. We note that only $\widetilde{R}_\uparrow(x)$ and $\widetilde{L}_\downarrow(x)$ are coupled, which leads to the opening of a gap, as shown in Fig. 3(b). This is similar to the spin-selective Peierls mechanism discovered in Ref. 39 where interaction effects strongly renormalize this gap (here, however, we shall ignore interaction effects).

The superconductivity term [see Eq. (7)] in the linearized model becomes

$$\widetilde{H}^{sc} = \frac{1}{2}\int dx\, \Delta_{sc}(\widetilde{R}_\uparrow(x)\widetilde{L}_\downarrow(x) - \widetilde{L}_\downarrow(x)\widetilde{R}_\uparrow(x)$$
$$+ \widetilde{L}_\uparrow(x)\widetilde{R}_\downarrow(x) - \widetilde{R}_\downarrow(x)\widetilde{L}_\uparrow(x) + \mathrm{H.c.}). \tag{14}$$

We construct two vectors, $\widetilde{\phi}^{(i)} = (\widetilde{R}_\uparrow, \widetilde{L}_\downarrow, \widetilde{R}_\uparrow^\dagger, \widetilde{L}_\downarrow^\dagger)$ and $\widetilde{\phi}^{(e)} = (\widetilde{L}_\uparrow, \widetilde{R}_\downarrow, \widetilde{L}_\uparrow^\dagger, \widetilde{R}_\downarrow^\dagger)$, which correspond to the exterior ($k \simeq 2k_{so}$) and interior ($k \simeq 0$) branches of the spectrum in the laboratory frame [see Fig. 3(a)]. The linearized Hamiltonian $\widetilde{H}^{\mathrm{kin}} + \widetilde{H}^Z + \widetilde{H}^{sc}$ reduces then to ($l = i,e$)

$$\widetilde{H}^{(l)} = \frac{1}{2}\int dx\, [\widetilde{\phi}^{(l)}(x)]^\dagger \widetilde{\mathcal{H}}^{(l)}\widetilde{\phi}^{(l)}(x), \tag{15}$$

where the interior branches are described by

$$\widetilde{\mathcal{H}}^{(i)} = -i\hbar\upsilon_F\sigma_3\partial_x + \Delta_z\sigma_1\eta_3 + \Delta_{sc}\sigma_2\eta_2, \tag{16}$$

and the exterior ones by

$$\widetilde{\mathcal{H}}^{(e)} = i\hbar\upsilon_F\sigma_3\partial_x + \Delta_{sc}\sigma_2\eta_2. \tag{17}$$

Here, the Pauli matrices $\eta_{1,2,3}$ act on the electron-hole subspace.

The energy spectrum is determined by the Schrödinger equation, $\widetilde{\mathcal{H}}^{(l)}\widetilde{\varphi}_E^{(l)}(x) = E\widetilde{\varphi}_E^{(l)}(x)$, with boundary conditions to be imposed on the eigenfunctions $\widetilde{\varphi}_E^{(l)}(x)$ as discussed below. We introduce then the operator $\widetilde{\gamma}_E^{(l)} = \int dx\, \widetilde{\varphi}_E^{(l)}(x) \cdot \widetilde{\phi}^{(l)}(x)$ and see that it diagonalizes Eq. (15), i.e., $\widetilde{H}^{(l)} = \sum_E E(\widetilde{\gamma}_E^{(l)})^\dagger\widetilde{\gamma}_E^{(l)}$.

Focusing now on the zero modes, we consider in particular $\widetilde{\gamma}^{(l)} \equiv \widetilde{\gamma}_{E=0}^{(l)}$ but express it in a more convenient basis,

$$\widetilde{\gamma}^{(l)} = \int dx \, \widetilde{\Phi}_{E=0}^{(l)}(x) \cdot \widetilde{\Psi}(x), \qquad (18)$$

where $\widetilde{\Psi} = (\widetilde{\Psi}_\uparrow, \widetilde{\Psi}_\downarrow, \widetilde{\Psi}_\uparrow^\dagger, \widetilde{\Psi}_\downarrow^\dagger)$ and where fast oscillating terms were dropped. In this new basis $\widetilde{\Psi}$, we have reinstalled the phase factors $e^{\pm i k_{so} x}$ (associated with $\widetilde{R}_\sigma$ and $\widetilde{L}_\sigma$) explicitly in the wave functions $\widetilde{\Phi}_{E=0}^{(l)}(x)$, so that they are taken automatically into account when we impose the boundary conditions on $\widetilde{\Phi}_{E=0}^{(l)}(x)$.

The zero-energy operator $\widetilde{\gamma}^{(l)}$ represents a MF, i.e., $(\widetilde{\gamma}^{(l)})^\dagger = \widetilde{\gamma}^{(l)}$, if and only if the corresponding wave function $\widetilde{\Phi}_{E=0}^{(l)}(x)$ has the following form:

$$\widetilde{\Phi}_{E=0}^{(l)}(x) = \begin{pmatrix} f(x) \\ g(x) \\ f^*(x) \\ g^*(x) \end{pmatrix}, \qquad (19)$$

where the functions f, g are arbitrary up to normalization $\int dx |\widetilde{\Phi}_{E=0}^{(l)}(x)|^2 / 2 = \int dx (|f(x)|^2 + |g(x)|^2) = 1$, which, however, will be suppressed in the following.

In infinite space (no boundary conditions), the spectrum of the interior branches [see Eq. (16)] is given by $E_\pm^{(i)} = \pm \sqrt{(\hbar \upsilon_F \kappa)^2 + \Delta_\pm^2}$, while the one for the exterior branches [see Eq. (17)] is given by $E_{1,2}^{(e)} = \pm \sqrt{(\hbar \upsilon_F \kappa)^2 + \Delta_e^2}$, where κ is taken from the Fermi point. Here, $\Delta_\pm = \Delta_{sc} \pm \Delta_Z$ and $\Delta_e = \Delta_{sc}$. If Δ_Z and Δ_{sc} become equal, the topological interior gap Δ_- is closed. In contrast, the exterior gap Δ_e is not affected by the magnetic field.

The only normalizable eigenstates of $\widetilde{\mathcal{H}}^{(l)}$ at zero energy and at $x > 0$ are two evanescent modes coming from the interior branches, characterized by a decay wave vector $k_\pm^{(i)} = |\Delta_\pm| / \alpha_R$, and two evanescent modes coming from the exterior branches, characterized by a decay wave vector $k^{(e)} = \Delta_{sc} / \alpha_R$. The corresponding zero-energy eigenfunctions $\widetilde{\varphi}_{E=0}^{(l)}(x)$ give the four basis wave functions, exponentially decaying in the semi-infinite space $x > 0$,

$$\widetilde{\Phi}_-^{(i)} = \begin{pmatrix} -i \, \text{sgn}(\Delta_-) e^{-ik_{so}x} \\ e^{ik_{so}x} \\ i \, \text{sgn}(\Delta_-) e^{ik_{so}x} \\ e^{-ik_{so}x} \end{pmatrix} e^{-k_-^{(i)}x},$$

$$(20)$$

$$\widetilde{\Phi}_+^{(i)} = \begin{pmatrix} e^{-ik_{so}x} \\ -i \, e^{ik_{so}x} \\ e^{ik_{so}x} \\ i \, e^{-ik_{so}x} \end{pmatrix} e^{-k_+^{(i)}x},$$

$$\widetilde{\Phi}_1^{(e)} = \begin{pmatrix} i \, e^{ik_{so}x} \\ e^{-ik_{so}x} \\ -i \, e^{-ik_{so}x} \\ e^{ik_{so}x} \end{pmatrix} e^{-k^{(e)}x}, \quad \widetilde{\Phi}_2^{(e)} = \begin{pmatrix} e^{ik_{so}x} \\ i \, e^{-ik_{so}x} \\ e^{-ik_{so}x} \\ -i \, e^{ik_{so}x} \end{pmatrix} e^{-k^{(e)}x}.$$

$$(21)$$

Here we should note that these four degenerate MF wave functions are not yet solutions of our problem: they do satisfy the Schrödinger equation but not yet the boundary conditions. Thus we search now for a linear combination of them, $\widetilde{\Phi}_M$, such that the boundary conditions are satisfied. At the left end of the nanowire, the condition on the wave function is $\widetilde{\Phi}_M(x=0) = 0$. We assume here that the length of the nanowire L_{sc} provides the largest scale, so we can neglect any interplay between the two ends of the nanowire and treat them independently (see also below). The set of vectors $\{\widetilde{\Phi}_-^{(i)}, \widetilde{\Phi}_+^{(i)}, \widetilde{\Phi}_1^{(e)}, \widetilde{\Phi}_2^{(e)}\}$ is seen to be linearly independent in the nontopological phase at $x = 0$, thus it is impossible to satisfy the boundary conditions and no solution exists at zero energy. In contrast, in the topological phase, $\Delta_Z > \Delta_{sc}$, the two vectors $\widetilde{\Phi}_-^{(i)}$ and $\widetilde{\Phi}_1^{(e)}$ are "collinear: such that the boundary condition can be satisfied and the zero energy state is a MF given by $\widetilde{\Phi}_M = \widetilde{\Phi}_-^{(i)} - \widetilde{\Phi}_1^{(e)}$ in the rotating frame. Using Eq. (9), the MF wave function in the laboratory frame is then given by

$$\Phi_M(x) = \begin{pmatrix} i \\ 1 \\ -i \\ 1 \end{pmatrix} e^{-k_-^{(i)}x} - \begin{pmatrix} i \, e^{ik_Fx} \\ e^{-ik_Fx} \\ -i \, e^{-ik_Fx} \\ e^{ik_Fx} \end{pmatrix} e^{-k^{(e)}x}, \qquad (22)$$

with $k_F = 2k_{so}$.

There are a few remarks in order. First, we see that the initial fourfold degeneracy of the MF has been completely removed by the boundary condition and we end up with one single nondegenerate MF wave function at the left end of the nanowire, $x = 0$ (analogously for the right end, $x = L_{sc}$). This is reminiscent of a well-known fact in elementary quantum mechanics, where for spinless particles in a one-dimensional box the degeneracy also gets removed by vanishing boundary conditions (whereas there is degeneracy for periodic boundary conditions).[40] This nondegeneracy of the MFs is a generic feature which will occur in all cases considered in this work, even in the presence of additional symmetries such as pseudotime-reversal invariance (see Sec. III B below and Ref. [41]).

Second, we see that the MF wave function Φ_M is a "composite" object that is a superposition of two MF wave functions with (essentially) disjoint supports in k space, one coming from the exterior ($\widetilde{\Phi}_1^{(e)}$) and one from interior ($\widetilde{\Phi}_-^{(i)}$) branches of the spectrum, respectively. Note that the corresponding wave vectors are extrema of the particle-hole spectrum shown in Fig. 2(b). As a consequence, these two MF wave functions have different localization lengths in real space, $\xi^{(i)} = 1/k_-^{(i)}$ and $\xi^{(e)} = 1/k^{(e)}$, which are inverse proportional to the corresponding gaps, $|\Delta_-|$ and Δ_{sc}. Which one of them determines the localization length of Φ_M depends on the ratio between Δ_Z and Δ_{sc}.

In particular, as the magnetic field is being increased from zero to the critical value $B_c = 2\Delta_{sc}/g\mu_B$, MFs emerge at each end of the nanowire.[5,7,8] However, if the localization lengths $\xi^{(i)}$ of these emerging MFs are comparable to the length L_{sc} of the nanowire, then these two MFs are hybridized into a subgap fermion of finite energy (see Appendix A). This then implies that the MFs in a finite wire can only appear at a magnetic field
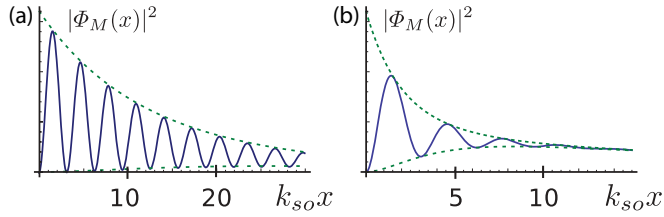
FIG. 4. (Color online) The MF probability density $|\Phi_M(x)|^2$, see Eq. (22), for a nanowire in the strong SOI regime with $\hbar^2 \Delta_{sc}/m\alpha_R^2 = 0.1$. The decaying MF wave function Φ_M oscillates with a period π/k_{so}. (a) In the topological phase but still near the transition, $\Delta_Z = 2\Delta_{sc}$, the MF wave function undergoes many oscillations due to the interference between $\widetilde{\Phi}^{(i)}$ and $\widetilde{\Phi}_1^{(e)}$. (b) Deep inside the topological phase, $\Delta_Z = 7\Delta_{sc}$, the MF wave function from the interior branches decays much faster than the one from the exterior branches. This leads to only a few oscillations of the density and a uniform decay with a decay wave vector $k^{(e)}$ away from the end of the nanowire.

$B_c^* \simeq B_c(1 + 4\alpha_R/\Delta_{sc}L_{sc})$ that is *larger* than the B_c obtained for a semi-infinite nanowire. If the magnetic field is increased further, the main contribution to the MF bound state comes from the exterior branches.

The composite structure of the MF wave function manifests itself in the probability density $|\Phi_M(x)|^2$ along the nanowire. The density of a MF coming only from one of the branches, for example, $\widetilde{\Phi}_-^{(i)}$, is just decaying exponentially. In contrast, the density of the composite MF exhibits oscillations (see Fig. 4). These oscillations are due to interference and are most pronounced when the contributions of $\widetilde{\Phi}_1^{(e)}$ and $\widetilde{\Phi}_-^{(i)}$ to $\widetilde{\Phi}_M$ are similar, i.e., when both decay lengths, $\xi^{(i)}$ and $\xi^{(e)}$, are close to each other.

The approach of the rotating magnetic field allows us to understand the structure of composite MF wave function. However, this approach is valid under the assumption that the SOI at the Fermi level is the largest energy scale. In order to explore the weak SOI regime, we come back to the full quadratic Hamiltonian in the next subsection.

B. Weak SOI regime: Near the topological phase transition

The regime of weak SOI is defined by the condition that the Zeeman splitting is much larger than the SOI energy at the Fermi level, $\Delta_Z \gg m\alpha_R^2/\hbar^2$ [or $k_F \approx k_Z$; see Eq. (6)]. This allows us to treat the SOI as a perturbation.[15,26]

Around the Fermi points, $\pm k_F$, the eigenstates of $\mathcal{H}^0$ are found from the Schrödinger equation $\mathcal{H}^0(-i\partial_x \to \pm k_F)\varphi^{R/L} = 0$ [see Eq. (4)] and given by

$$\varphi_0^{R/L} = \frac{1}{\sqrt{2}}\begin{pmatrix} -1 \pm \frac{k_{so}}{k_F} \\ 1 \pm \frac{k_{so}}{k_F} \end{pmatrix}, \qquad (23)$$

where $\varphi_0^{R/L}$ denotes the eigenstates at $k = \pm k_F$. In Eq. (23) we kept only terms up to first order in k_{so}/k_F. As expected, φ_0^R and φ_0^L are nearly "aligned" along the magnetic field since $\Delta_Z \gg \alpha_R k_F$. In the absence of SOI, φ_0^R and φ_0^L are perfectly aligned along the x axis and have the same spin, so they cannot be coupled by an ordinary s-wave superconductor. The SOI slightly tilts the spins in the orthogonal direction, which then allows the coupling between these states if the nanowire is brought into the proximity of an s-wave superconductor.

The exterior branches can be treated in the linearized approximation similar to Sec. III A,

$$\chi(x) = R(x)e^{ik_Fx} + L(x)e^{-ik_Fx}, \qquad (24)$$

where, again, R (L) annihilates a right- (left-) moving electron. These operators are connected to spin-up ($\Psi_\uparrow$) and spin-down ($\Psi_\downarrow$) electron operators as $R(x) = \varphi^R(x) \cdot \psi$ and $L(x) = \varphi^L(x) \cdot \psi$, where $\psi = (\Psi_\uparrow, \Psi_\downarrow)$ (with corresponding support for right and left movers). Here, $\varphi^{R/L}(x)$ is given by Eq. (23) but where we allow now also for a slowly varying x dependence.

In this approximation, we find

$$H^0 = -i\hbar\upsilon_F \int dx \, [R^\dagger(x)\partial_x R(x) - L^\dagger(x)\partial_x L(x)], \qquad (25)$$

where the Fermi velocity is given by $\upsilon_F \approx \sqrt{2\Delta_Z/m}$. The proximity-induced superconductivity [see Eq. (7)] is described in the linearized model as

$$H^{sc} = \frac{1}{2}\int dx \, \overline{\Delta}_{sc}(R(x)L(x) - L(x)R(x) + \text{H.c.}), \qquad (26)$$

where the strength of the proximity-induced effective p-wave superconductivity, $\overline{\Delta}_{sc}$, is found from Eqs. (7), (23), and (24),

$$\frac{\overline{\Delta}_{sc}}{\Delta_{sc}} = \left(\varphi_0^R\right)^* \cdot i\sigma_2\varphi_0^L = 2\frac{k_{so}}{k_F} = \frac{\sqrt{2m}\alpha_R}{\hbar\sqrt{\Delta_Z}} \ll 1. \qquad (27)$$

The suppression of $\overline{\Delta}_{sc}$ compared to Δ_{sc} can be understood from the fact that two states with opposite momenta at the Fermi level have mostly parallel spins due to the strong magnetic field and they slightly deviate in the orthogonal direction due to the weak SOI, which then leads to a suppression of Δ_{sc} by a factor k_{so}/k_F.

Again, introducing a vector $\phi^{(e)}(x) = (R, L, R^\dagger, L^\dagger)$, we represent the linearized Hamiltonian $H^{(e)} = H^0 + H^{sc}$ as

$$H^{(e)} = \frac{1}{2}\int dx (\phi^{(e)})^\dagger \mathcal{H}^{(e)}\phi^{(e)},$$
$$\mathcal{H}^{(e)} = -i\hbar\upsilon_F\tau_3\partial_x + \overline{\Delta}_{sc}\tau_2\eta_2, \qquad (28)$$

where the Pauli matrices $\tau_{1,2,3}$ act on the right-/left-mover subspace.

The spectrum around the Fermi points in infinite space (no boundary conditions) follows from the Schrödinger equation, $\mathcal{H}^{(e)}\varphi^{(e)} = E^{(e)}\varphi^{(e)}$, and is given by $E_{1,2}^{(e)} = \pm\sqrt{(\hbar\upsilon_F\kappa)^2 + \Delta_e^2}$, where the momentum κ is again taken from the Fermi points. Here, $2\Delta_e \equiv 2\overline{\Delta}_{sc}$ is the gap induced by superconductivity.

The zero-energy solutions that are normalizable for $x > 0$ are two evanescent modes with wave vector $\bar{k}^{(e)} = \overline{\Delta}_{sc}/\hbar\upsilon_F$ determining the localization length. These solutions can be written explicitly as $\varphi_1^{(e)} = (1, -i, 1, i)e^{-\bar{k}^{(e)}x}$ and $\varphi_2^{(e)} = (-i, 1, i, 1)e^{-\bar{k}^{(e)}x}$. Repeating the procedure that led us to Eq. (18) in Sec. III A, we can introduce a new MF operator,

$$\gamma = \int dx \, \Phi_{E=0}(x) \cdot \Psi(x). \qquad (29)$$

Here $\Psi = (\Psi_\uparrow, \Psi_\downarrow, \Psi_\uparrow^\dagger, \Psi_\downarrow^\dagger)$. The two corresponding wave functions are written as

$$\Phi_j^{(e)} = \begin{pmatrix} f_j(x) \\ i f_j^*(x) \\ f_j^*(x) \\ -i f_j(x) \end{pmatrix} e^{-\bar{k}^{(e)} x}, \tag{30}$$

where

$$
\begin{aligned}
f_1(x) &= i(1 + k_{so}/k_F) e^{ik_F x} - (1 - k_{so}/k_F) e^{-ik_F x}, \\
f_2(x) &= i(1 - k_{so}/k_F) e^{-ik_F x} - (1 + k_{so}/k_F) e^{ik_F x}.
\end{aligned} \tag{31}
$$

The effect of the SOI on the states around $k = 0$ is negligible near the topological phase transition if $\hbar^2 |\Delta_-|/2m\alpha_R^2 \ll 1$. Therefore the eigenstates for weak and strong SOIs are the same in first order in SOI. This means that we are allowed to take $\widetilde{\Phi}_-^{(i)}$ and $\widetilde{\Phi}_+^{(i)}$ given by Eq. (20) and transform them back into the laboratory frame,

$$\Phi_-^{(i)} = \begin{pmatrix} -i\,\text{sgn}(\Delta_-) \\ 1 \\ i\,\text{sgn}(\Delta_-) \\ 1 \end{pmatrix} e^{-k_-^{(i)} x}, \quad \Phi_+^{(i)} = \begin{pmatrix} 1 \\ -i \\ 1 \\ i \end{pmatrix} e^{-k_+^{(i)} x}. \tag{32}$$

After we found four basis wave functions $\{\Phi_-^{(i)}, \Phi_+^{(i)}, \Phi_1^{(e)}, \Phi_2^{(e)}\}$, we should impose the boundary conditions on their linear combination $\Phi(x)$. The wave function $\Phi(x)$ should vanish at the boundary $x = 0$. One can see that if we neglect the corrections to the wave functions $\Phi_1^{(e)}$ and $\Phi_2^{(e)}$ coming from SOI, then we are able to satisfy the boundary conditions. This is a consequence of the fact that in the absence of SOI both states at the Fermi level have the same spin, so that the functions $\Phi_i^{(e)}$, $i = 1, 2$, effectively become spinless objects and the MF always exists and arises only from the exterior branches. For the complete treatment, however, we should also consider contributions from the interior branches. This will be addressed next.

The set of wave functions $\{\Phi_-^{(i)}, \Phi_+^{(i)}, \Phi_1^{(e)}, \Phi_2^{(e)}\}$ becomes linearly dependent in the topological regime $\Delta_- < 0$ and the MF wave function is given by

$$\Phi_M = \left(1 - \frac{k_{so}}{k_F}\right) \Phi_1^{(e)} - \left(1 - \frac{k_{so}}{k_F}\right) \Phi_2^{(e)} - 4\frac{k_{so}}{k_F} \Phi_-^{(i)}. \tag{33}$$

As in the regime of strong SOI (see Sec. III A), the MF wave function has its support around wave vectors $k = 0$ (interior branches) and $k = \pm k_F$ (exterior branches). However, in contrast to the previous case, the contribution of the interior branches is suppressed by the small parameter k_{so}/k_F, thus the exterior branches contribute most to the MF wave function. At the same time we note that the localization length of MFs is determined by the smallest gap in the system. Near the topological phase transition,[7,8] which corresponds to the closing of the topological (interior) gap, the interior branches determine the localization length as long as $\bar{k}^{(e)} > k_-^{(i)}$. If the magnetic field is increased further, the gap in the system is given by the exterior gap, $2\Delta_e = 2\bar{\Delta}_{sc} \propto 1/\sqrt{B}$ [see Eq. (27)]. The localization length is increasing as $\propto B$. As soon as it is comparable to the nanowire length L_{sc}, the wave function of
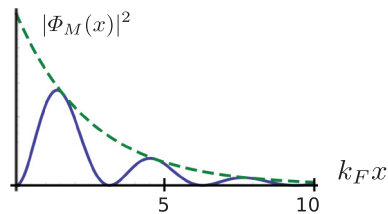

FIG. 5. (Color online) The MF probability density $|\Phi_M(x)|^2$ for a nanowire in the weak SOI regime ($m\alpha_R^2/\hbar^2 \Delta_{sc} = 0.2$ and $\Delta_Z = 5\Delta_{sc}$) oscillates with period π/k_F due to interference between right- and left-moving contributions [see Eq. (30)]. The decay length is given by $1/\bar{k}^{(e)}$.

the two MFs at opposite ends overlap, and the two zero-energy MF levels are split into one subgap fermion of finite energy.

In the weak SOI regime and sufficiently far away from the topological transition point, $\Delta_Z > \Delta_{sc}(1 + k_{so}/k_F)$, so that the gap is determined by the exterior branches only, we can work in the simplified model[15] given by $\mathcal{H}^{(e)}$ [see Eq. (28)]. The explicit MF wave function can be found from Eq. (33),

$$\Phi_M(x) = \begin{pmatrix} e^{-i\pi/4} \\ i e^{i\pi/4} \\ e^{i\pi/4} \\ -i e^{-i\pi/4} \end{pmatrix} \sin(k_F x) e^{-\bar{k}^{(e)} x}. \tag{34}$$

Again, we note that this wave function describes a MF with the spin of both, the electron and the hole, pointing in the x direction, again, up to corrections of order of k_{so}/k_F. The MF probability density $|\Phi_M(x)|^2 \propto \sin^2(k_F x) e^{-2\bar{k}^{(e)} x}$ decays oscillating with a period half the Fermi wavelength, $\lambda_F/2 = \pi/k_F$ (see Fig. 5). In passing, we remark that $\mathcal{H}^{(e)}$ given in Eq. (28) belongs to the topological class DIII according to the classification scheme of Ref. 42 and supports MFs in one dimension, in agreement with our result Eq. (34).[41]

IV. MAJORANA FERMIONS IN NS JUNCTIONS

In this section we consider a nanowire containing a normal-superconducting (NS) junction where the right part is in the superconducting and the left part in the normal regime; see Fig. 6. The junction is assumed to be fully transparent. We will show that the MF wave function leaks out of the superconducting section and leads to a new MF bound state
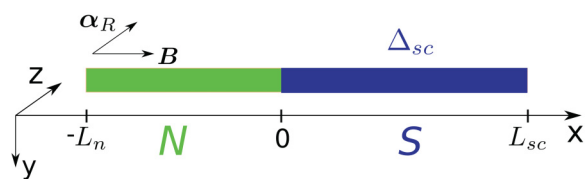

FIG. 6. (Color online) NS junction of a nanowire. The right section (blue) of the nanowire from $x = 0$ to $x = L_{sc}$ is brought into contact with a bulk s-wave superconductor (not shown) that induces a gap Δ_{sc} in the nanowire via proximity effect. The left section (green) of the nanowire from $x = -L_n$ to $x = 0$ is in the normal regime. A magnetic field **B** is applied along the entire nanowire in x direction and perpendicularly to the Rashba SOI vector α_R, which points in z direction.

that extends over the entire normal section. We note that this bound state is different from Andreev bound states[44] known to occur in NS junction systems. Indeed, the existence of the latter at zero energy would be accidental in the presence of a magnetic field since they move away from the Fermi level if the magnetic field is varied. Further, the MFs found in this section always exist in the topological regime and are not sensitive to the length L_n of the normal section, in stark contrast to Andreev bound states that move in energy as a function of L_n.[44,45]

We continue to work with the formalism developed in Sec. III [see Eqs. (18) and (29)] and represent γ in the basis of electron/hole spin-up/spin-down operators $\Psi(x)$ in terms of a four-component vector $\Phi(x)$ on which we impose the boundary conditions. As before, the length of the superconducting part of the nanowire L_{sc} is assumed to be much larger than any decay length given by $k_-^{(i)}$, $k_+^{(i)}$, or $k^{(e)}$ ($\bar{k}^{(e)}$). This assumption allows us to treat the nanowire again as semi-infinite with no boundary conditions at $x = L_{sc}$. In contrast, the normal section, $x \in [-L_n, 0]$, is finite. Thus at $x = 0$ we invoke continuity of the wave functions and of their derivatives[46] and at $x = -L_n$ we impose vanishing boundary conditions,

$$\Phi(x = 0^-) = \Phi(x = 0^+), \qquad (35)$$

$$\partial_x \Phi(x = 0^-) = \partial_x \Phi(x = 0^+), \qquad (36)$$

$$\Phi(x = -L_n) = 0. \qquad (37)$$

The analytical form of the functions $\Phi(x)$ can be found in two regimes, again in the weak and strong SOI limits, which we address now in turn.

A. NS junction in the strong SOI regime

As before, the most convenient way to treat the strong SOI regime is to work in the rotating frame. In Sec. III A we already found the four basis wave functions at zero energy,

$$\left(\widetilde{\Phi}_1^{(sc)}, \widetilde{\Phi}_2^{(sc)}, \widetilde{\Phi}_3^{(sc)}, \widetilde{\Phi}_4^{(sc)}\right) = \left(\widetilde{\Phi}_-^{(i)}, \widetilde{\Phi}_+^{(i)}, \widetilde{\Phi}_1^{(e)}, \widetilde{\Phi}_2^{(e)}\right), \quad (38)$$

in the superconducting section, for $x \geqslant 0$ [see Eqs. (20) and (21)].

The eigenfunctions for the normal section can be found from the linearized Hamiltonians for the interior branches, $\widetilde{\mathcal{H}}^{(i)}$ [see Eq. (16)], and for the exterior branches, $\widetilde{\mathcal{H}}^{(e)}$ [see Eq. (17)], with $\Delta_{sc} = 0$. The exterior branches are not gapped leading to the four propagating modes [see Fig. 3(b)] with wave functions given by

$$\widetilde{\Phi}_1^{(n)} = \begin{pmatrix} -i\, e^{ik_{so}x} \\ e^{-ik_{so}x} \\ i\, e^{-ik_{so}x} \\ e^{ik_{so}x} \end{pmatrix}, \quad \widetilde{\Phi}_2^{(n)} = \begin{pmatrix} e^{ik_{so}x} \\ i\, e^{-ik_{so}x} \\ e^{-ik_{so}x} \\ -i\, e^{ik_{so}x} \end{pmatrix},$$

$$\widetilde{\Phi}_3^{(n)} = \begin{pmatrix} i\, e^{ik_{so}x} \\ e^{-ik_{so}x} \\ -i\, e^{-ik_{so}x} \\ e^{ik_{so}x} \end{pmatrix}, \quad \widetilde{\Phi}_4^{(n)} = \begin{pmatrix} e^{ik_{so}x} \\ -i\, e^{-ik_{so}x} \\ e^{-ik_{so}x} \\ i\, e^{ik_{so}x} \end{pmatrix}, \qquad (39)$$

where we choose to represent the wave functions in form of MFs, guided by our expectation that the final solution is also a MF. The interior branches are gapped by the magnetic field [see Fig. 3(b)] and the four corresponding wave functions describing evanescent modes are given by

$$\widetilde{\Phi}_5^{(n)} = \begin{pmatrix} -i\, e^{-ik_{so}x} \\ e^{ik_{so}x} \\ i\, e^{ik_{so}x} \\ e^{-ik_{so}x} \end{pmatrix} e^{k^{(n)}x}, \quad \widetilde{\Phi}_6^{(n)} = \begin{pmatrix} e^{-ik_{so}x} \\ i\, e^{ik_{so}x} \\ e^{ik_{so}x} \\ -i\, e^{-ik_{so}x} \end{pmatrix} e^{k^{(n)}x},$$

$$(40)$$

$$\widetilde{\Phi}_7^{(n)} = \begin{pmatrix} i\, e^{-ik_{so}x} \\ e^{ik_{so}x} \\ -i\, e^{ik_{so}x} \\ e^{-ik_{so}x} \end{pmatrix} e^{-k^{(n)}(L_n+x)},$$

$$(41)$$

$$\widetilde{\Phi}_8^{(n)} = \begin{pmatrix} e^{-ik_{so}x} \\ -i\, e^{ik_{so}x} \\ e^{ik_{so}x} \\ i\, e^{-ik_{so}x} \end{pmatrix} e^{-k^{(n)}(L_n+x)},$$

with $k^{(n)} = \Delta_Z/\alpha_R$. The modes $\widetilde{\Phi}_{5,6}^{(n)}$ decay from their maximum at $x = 0$ to zero for $x \to -\infty$, while $\widetilde{\Phi}_{7,8}^{(n)}$ decay from their maximum at $x = -L_n$ to zero for $x \to +\infty$.

After having introduced the basis consisting of 12 MF wave functions given by Eqs. (20), (21), (39), and (41), we search for their linear combination,

$$\widetilde{\Phi}_M(x) = \begin{cases} \sum_{j=1}^{4} a_j \widetilde{\Phi}_j^{(sc)}, & x \geqslant 0, \\ \sum_{j=1}^{8} b_j \widetilde{\Phi}_j^{(n)}, & -L_n \leqslant x \leqslant 0, \end{cases} \qquad (42)$$

such that the boundary conditions (35)–(37) are satisfied. This is, in general, possible only in the topological phase. However, we also find solutions in the nontopological phase, where these solutions exist only if some special relations between the parameters Δ_Z, α_R, Δ_{sc}, and L_n are satisfied. This allows us to identify them as Andreev bound states in an NS junction. Since they are not of interest here, we focus on the solutions in the topological phase only.

It is worth of pointing out that due to the internal symmetry of the MF wave functions, five of the coefficients are readily seen to vanish, namely

$$a_2 = b_1 = b_4 = b_5 = b_8 = 0. \qquad (43)$$

The exact analytical solution is given in Appendix B and used for the plot in Fig. 7. Here, we only discuss the two limiting cases of long and short normal sections L_n.

First, we consider $L_n \gg 1/k^{(n)}$, allowing us to neglect the terms $\widetilde{\Phi}_5^{(n)}$ and $\widetilde{\Phi}_6^{(n)}$ at $x = -L_n$, and $\widetilde{\Phi}_7^{(n)}$ and $\widetilde{\Phi}_8^{(n)}$ at $x = 0$. In this case, the sum in Eq. (42) is determined by the coefficients

$$a_1 \to 0, \quad b_6 \to 0, \quad b_7 = -1,$$

$$a_3 = b_3 = \cos(2k_{so}L_n), \quad a_4 = b_2 = -\sin(2k_{so}L_n), \qquad (44)$$

leading to the solution of the form

$$
\widetilde{\Phi}_M(x) = \begin{cases} \widetilde{\Phi}_3^{(n)}(2L_n + x)\, e^{-k^{(e)}x}, & x > 0 \\ \widetilde{\Phi}_3^{(n)}(2L_n + x) - \widetilde{\Phi}_3^{(n)}(-x)\, e^{-k^{(n)}(x+L_n)}, & -L_n \leqslant x < 0. \end{cases}
\tag{45}
$$

Thus we see that the MF wave function in the laboratory frame, $\Phi_M(x)$, decays monotonically in the superconducting section while it oscillates in the normal one (see Fig. 7). In weak magnetic fields the MF probability density $|\Phi_M(x)|^2$ oscillates over the entire normal section, in contrast to the near absence of oscillations in strong magnetic fields.

We note that a long normal section serves as a "momentum filter." As shown in Sec. III A, a MF has equal support from the exterior and interior branches [see Eq. (22)] if the entire nanowire is in the superconducting regime. In contrast to that, if a significant portion of the nanowire is in the normal regime, the MF has support mostly from the exterior branches with momenta $k \simeq \pm k_F$. The contributions from the interior branches with momenta $k \simeq 0$ are negligibly small, $a_1 \to 0$ and $a_2 = 0$. This behavior can be understood in terms of momentum mismatch: the normal section does not have propagating modes with $k = 0$ (in the laboratory frame). Thus while such $k = 0$ modes exist in the superconducting section, they cannot propagate into the normal section.

Second, we consider the opposite limit $L_n \ll 1/k^{(n)}$. Here, we can treat the decaying solutions, $\widetilde{\Phi}_j^{(n)}$, $j = 5,6,7,8$, as being constant over L_n. The MF wave function $\widetilde{\Phi}_M(x)$ is constructed from seven basis MF wave functions with the same coefficients as in Eq. (44) with the only difference that now $a_1 = -1$. For short normal sections, the form of the MF
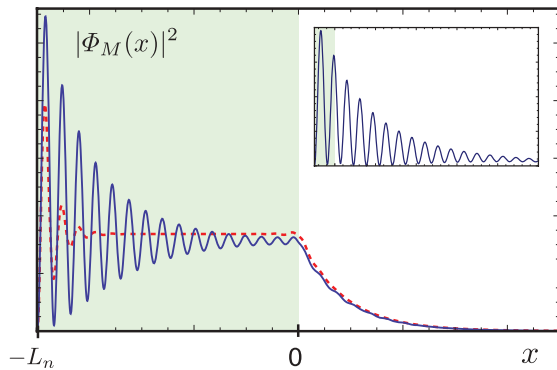

FIG. 7. (Color online) The MF probability density $|\Phi_M(x)|^2$ in an NS junction for a nanowire in the strong SOI regime ($\hbar^2 \Delta_{sc}/m\alpha_R^2 = 0.06$). The normal section of length L_n is long compared to the decay length, i.e., $k^{(n)}L_n \gg 1$. The MF wave function extends over the entire normal section (green) and decays exponentially inside the superconducting section (white). The oscillations with period π/k_{so} result from interference between the three components $\widetilde{\Phi}_{2,3,7}^{(n)}$, of Φ_M. In weak magnetic fields ($\Delta_Z = 1.5\Delta_{sc}$, blue full line), $k^{(n)}L_n \sim 1$, and the oscillations extend over the entire normal section. In contrast, in strong magnetic fields ($\Delta_Z = 7\Delta_{sc}$, red dashed line), the oscillations are strongly suppressed. Inset: $|\Phi_M(x)|^2$ as function of x for a short normal section, $k^{(n)}L_n \ll 1$. Similarly to the case of the superconducting wire (see Fig. 4), $|\Phi_M(x)|^2$ decays oscillating.

probability density $|\Phi_M(x)|^2$ is very similar to the one of a superconducting nanowire [compare the inset of Fig. 7 with Fig. 4(a)]. Again, the interference between $\widetilde{\Phi}_-^{(i)}$, $\widetilde{\Phi}_1^{(e)}$, and $\widetilde{\Phi}_2^{(e)}$ leads to oscillations in the superconducting section.

In both limits of short and long normal sections, $|\Phi_M(x)|^2$ has its maximum in the normal section while it decays in the superconducting one. This opens the possibility of measuring the presence of a MF state spectroscopically in the normal section. The amplitude and period of oscillations of the MF probability density is sensitive to magnetic fields and to the nanowire length, controlled, e.g., by an infinite barrier on the left end. Moreover, by shifting such a barrier via gates, we can change the type of MF from $\widetilde{\Phi}_1^{(e)}$ to $\widetilde{\Phi}_2^{(e)}$ [see Eqs. (38), (42), and (44)]. This amounts to changing a given MF state from a "real part" type, $\psi + \psi^\dagger$, to an "imaginary part" type, $i(\psi - \psi^\dagger)$.

B. NS junction in the weak SOI regime

As before, we first identify basis wave functions in the superconducting section and in the normal section. Then, we search for a linear combination of them such that the boundary conditions given by Eqs. (35)–(37) are satisfied.

As shown in Sec. III B, the MF wave function Φ_M has predominantly support from the exterior branches. The correction to the MF wave function from the interior branches is suppressed by a factor k_{so}/k_F [see Eq. (33)]. If we focus on the regime away from the topological phase transition where the exterior gap is smaller than the interior one, then, as in Eq. (30), the MF wave function can be constructed to first order in k_{so}/k_F from the exterior wave functions $\Phi_{j=1,2}^{(e)}$ alone,

$$
\Phi_j^{(sc)} = \begin{pmatrix} g_j(x) \\ i g_j^*(x) \\ g_j^*(x) \\ -i g_j(x) \end{pmatrix} e^{-\bar{k}^{(e)}x},
$$

$$
g_1 = e^{-i\pi/4}\sin(k_F x), \quad g_2 = e^{-i\pi/4}\cos(k_F x).
\tag{46}
$$

The propagating electron modes φ^R and φ^L of Eq. (23) in the normal section described by H^0 (without H^{sc}) were considered before [see Eq. (29)] and given by

$$
\Phi_1^{(n)} = \begin{pmatrix} e^{-ik_F x} \\ -e^{-ik_F x} \\ e^{ik_F x} \\ -e^{ik_F x} \end{pmatrix}, \quad
\Phi_2^{(n)} = \begin{pmatrix} e^{ik_F x} \\ -e^{ik_F x} \\ e^{-ik_F x} \\ -e^{-ik_F x} \end{pmatrix},
$$

$$
\Phi_3^{(n)} = \begin{pmatrix} i e^{-ik_F x} \\ -i e^{-ik_F x} \\ -i e^{ik_F x} \\ i e^{ik_F x} \end{pmatrix}, \quad
\Phi_4^{(n)} = \begin{pmatrix} i e^{ik_F x} \\ -i e^{ik_F x} \\ -i e^{-ik_F x} \\ i e^{-ik_F x} \end{pmatrix}.
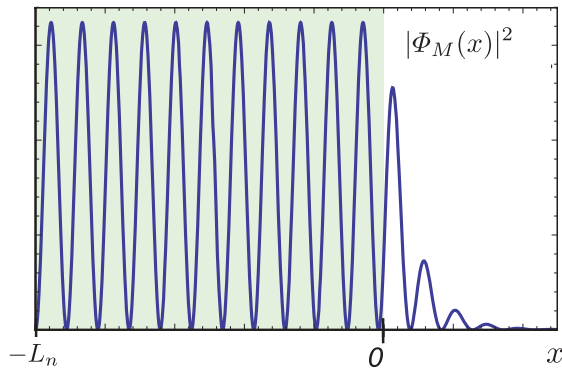\tag{47}
$$

FIG. 8. (Color online) The MF probability density $|\Phi_M(x)|^2$ in an NS junction for a nanowire in the weak SOI regime ($m\alpha_R^2/\hbar^2\Delta_{sc} = 0.2$ and $\Delta_Z = 5\Delta_{sc}$). The MF wave function extends over the entire normal section of length L_n (green) and decays rapidly inside the superconducting section (white).

The ansatz for the wave function in both sections is

$$\Phi(x) = \begin{cases} \sum_{j=1}^2 a_j \Phi_j^{(sc)}, & x \geqslant 0 \\ \sum_{j=1}^4 b_j \Phi_j^{(n)}, & -L_n \leqslant x \leqslant 0. \end{cases} \quad (48)$$

The coefficients a_j and b_j can then be found from the boundary conditions (35)–(37),

$$\begin{aligned} a_1 &= 2[\bar{k}^{(e)}\sin(k_F L_n) + k_F\cos(k_F L_n)], \\ a_2 &= 2k_F\sin(k_F L_n), \\ b_1 &= -b_4 = k_F\cos(k_F L_n - \pi/4), \\ b_2 &= -b_3 = -k_F\cos(k_F L_n + \pi/4), \end{aligned} \quad (49)$$

leading finally to the MF wave function of the form

$$\Phi_M(x) = f(x) \begin{pmatrix} e^{-i\pi/4} \\ -e^{-i\pi/4} \\ e^{i\pi/4} \\ -e^{i\pi/4} \end{pmatrix}, \quad (50)$$

where

$$f(x) = \begin{cases} k_F\sin(k_F[x+L_n]), & -L_n \leqslant x \leqslant 0, \\ e^{-\bar{k}^e x}[k_F\sin(k_F[x+L_n]) \\ \quad + \bar{k}^e\sin(k_F x)\sin(k_F L_n)], & x \geqslant 0. \end{cases} \quad (51)$$

The corresponding MF probability density $|\Phi_M(x)|^2$ is shown in Fig. 8. The MF wave function extends over the entire normal section. In this section, we considered as basis functions only propagating modes, $\Phi_j^{(n)}$, leading to a purely oscillatory solution with the period given by half the Fermi wavelength $\lambda_F/2 = \pi/k_F$. In contrast, in the superconducting section, the MF wave function decays on a short distance. In other words, the MF is mostly delocalized over the entire normal section and is strongly localized in the superconducting section, in agreement with recent numerical results.[38] This might simplify the detection of MFs by local-density measurements since the normal section is freely accessible to tunnel contacts, in contrast to the superconducting section which needs to be covered by a bulk s-wave superconductor.

V. CONCLUSIONS

In this work, we have focused on the wave-function properties of Majorana fermions occurring in superconducting nanowires and in nanowires with an NS junction. The superconducting phase is effectively p wave and is based on an interplay of s-wave proximity effect, spin-orbit interaction, and magnetic fields. We have derived explicit results for the MF wave functions in the regime of strong and weak SOI and shown that the wave functions are composite objects, being superpositions of contributions coming from the interior (around $k = 0$) and exterior (around $\pm k_F$) branches of the spectrum in momentum space. While the underlying Hamiltonians considered in this work allow degenerate MF wave functions, the boundary conditions at hand completely lift this degeneracy and we are left with only one single MF state at a given end of the nanowire (i.e., in total there are two MF states for the entire nanowire).

In the strong SOI regime of a superconducting nanowire both branches contribute equally. However, the decay length of the MF is determined by the branch that also defines the smallest gap in the system. Moreover, the oscillations in the MF probability density with period of the Fermi wavelength are decaying on the scale given by the largest gap in the system. In the weak SOI regime, the exterior branches mostly contribute to the MF wave function. The contributions of the interior branch are suppressed by the small factor $k_{so}/k_F \ll 1$ and only close to the topological phase transition does this branch determine the localization length of the MF. The interference between modes from k_F and $-k_F$ leads to oscillations of the probability density of the MF with an exponentially decaying envelope.

For a nanowire with an NS junction we find that the MF wave function becomes delocalized over the entire normal section, while still being localized in the superconducting section, in agreement with recent numerical results.[38] Again, we obtain analytical results for the weak and strong SOI regimes. Depending on the length of the normal section, the support of the MF wave function is centered at zero momentum or at the Fermi points. Again, we find different localization lengths and oscillation periods of the MF in the normal section that are tunable by magnetic fields. Based on this insight, we expect that in a tunneling density of states measurement the tunneling current at zero bias exhibits oscillations as a function of position along the normal section due to the presence of the MF in the normal section.

Finally, we remark that in this work we have focused on single-particle properties and ignored, in particular, interaction effects. It would be interesting to extend the present analysis to interacting Luttinger liquids, in particular for the SOI nanowire with an NS junction, combining the approaches developed in Refs. 14, 15, 39, and 47.

APPENDIX A: FINITE NANOWIRE

In this Appendix we address the problem of a finite superconducting section of length L_{sc}. In this case, the decaying modes $\widetilde{\Phi}_0 = \{\widetilde{\Phi}_-^{(i)}, \widetilde{\Phi}_+^{(i)}, \widetilde{\Phi}_1^{(e)}, \widetilde{\Phi}_2^{(e)}\}$ with maximum at $x = 0$ are given by Eqs. (20) and (21). Now we should also take into account the four evanescent modes with maximum at $x = L_{sc}$. These modes, $\widetilde{\Phi}_{L_{sc}} = \{\widetilde{\Phi}_-^{(i)}, \widetilde{\Phi}_+^{(i)}, \widetilde{\Phi}_1^{(e)}, \widetilde{\Phi}_2^{(e)}\}$, are found from Eqs. (16) and (17) and are similar by their structure to $\widetilde{\Phi}_0$,

$$\widetilde{\Phi}_-^{(i)} = \begin{pmatrix} i\,\mathrm{sgn}(\Delta_-)e^{-ik_{\mathrm{so}}x} \\ e^{ik_{\mathrm{so}}x} \\ -i\,\mathrm{sgn}(\Delta_-)e^{ik_{\mathrm{so}}x} \\ e^{-ik_{\mathrm{so}}x} \end{pmatrix} e^{k_-^{(i)}(x-L_{sc})}, \quad \widetilde{\Phi}_+^{(i)} = \begin{pmatrix} e^{-ik_{\mathrm{so}}x} \\ i\,e^{ik_{\mathrm{so}}x} \\ e^{ik_{\mathrm{so}}x} \\ -i\,e^{-ik_{\mathrm{so}}x} \end{pmatrix} e^{-k_+^{(i)}(x-L_{sc})},$$

$$\widetilde{\Phi}_1^{(e)} = \begin{pmatrix} -i\,e^{ik_{\mathrm{so}}x} \\ e^{-ik_{\mathrm{so}}x} \\ i\,e^{-ik_{\mathrm{so}}x} \\ e^{ik_{\mathrm{so}}x} \end{pmatrix} e^{-k^{(e)}(x-L_{sc})}, \quad \widetilde{\Phi}_2^{(e)} = \begin{pmatrix} e^{ik_{\mathrm{so}}x} \\ -i\,e^{-ik_{\mathrm{so}}x} \\ e^{-ik_{\mathrm{so}}x} \\ i\,e^{ik_{\mathrm{so}}x} \end{pmatrix} e^{-k^{(e)}(x-L_{sc})}. \tag{A1}$$

We construct an 8×4 matrix $\widetilde{\omega}(x)$ from the eight basis wave functions. The zero-energy solution can then be compactly written as

$$\widetilde{\Phi}(x) = \mathbf{a} \cdot \widetilde{\Phi}_0(x) + \mathbf{b} \cdot \widetilde{\Phi}_{L_{sc}}(x) \equiv \widetilde{\omega}(x)\begin{pmatrix} \mathbf{a} \\ \mathbf{b} \end{pmatrix}, \tag{A2}$$

where $\mathbf{a} = (a_1, a_2, a_3, a_4)$ and $\mathbf{b} = (b_1, b_2, b_3, b_4)$ are coefficients that should be determined from the boundary conditions,

$$\widetilde{\Phi}(x = 0, L_{sc}) = 0, \tag{A3}$$

which can be rewritten as a matrix equation in terms of an 8×8 matrix $\widetilde{\Omega}$,

$$\widetilde{\Omega}\begin{pmatrix} \mathbf{a} \\ \mathbf{b} \end{pmatrix} = (\widetilde{\omega}(0)\ \widetilde{\omega}(L_{sc}))\begin{pmatrix} \mathbf{a} \\ \mathbf{b} \end{pmatrix} = 0. \tag{A4}$$

The determinant of the matrix $\widetilde{\Omega}$ is nonzero, so the solution of the matrix equation is unique and trivial, $(\mathbf{a}, \mathbf{b}) = 0$. This means that, strictly speaking, MFs cannot emerge in a finite-size nanowire. MFs exist only under the assumption that the overlap of the two MF wave functions (localized at each end of the nanowire and derived in a semi-infinite nanowire model) can be neglected. Otherwise, the two MFs are hybridized into a subgap fermion of finite energy.

APPENDIX B: EXACT SOLUTION IN STRONG SOI REGIME

Here, we present the exact solution for the MF wave function $\widetilde{\Phi}(x)$ composed of seven different basis MFs wave functions [see Eq. (42)] and satisfying the boundary conditions (35)–(37). We find

$a_2 = b_1 = b_4 = b_5 = b_8 = 0,$

$a_1 = 4k_{\mathrm{so}}^2 + 4k_{\mathrm{so}}k^{(e)}\cosh(k^{(n)}L)\sin(2k_{\mathrm{so}}L_n) - 2k^{(e)}\cos(2k_{\mathrm{so}}L_n)[k^{(e)}\cosh(k^{(n)}L_n) + k^{(n)}\sinh(k^{(n)}L_n)],$

$a_3 = e^{-k^{(n)}L_n}\{e^{k^{(n)}L_n}(k^{(e)}[k^{(n)} - 2k_-^{(i)}] + k^{(n)}[k^{(n)} - k_-^{(i)}]) - 4k_{\mathrm{so}}^2 e^{2k^{(n)}L_n}\cos(2k_{\mathrm{so}}L_n) - 2k_{\mathrm{so}}(e^{2k^{(n)}L_n}k^{(e)} + k_-^{(i)} - k^{(n)})\sin(2k_{\mathrm{so}}L_n)\},$

$a_4 = -e^{-k^{(n)}L_n}[2e^{k^{(n)}L_n}k_{\mathrm{so}}(k^{(n)} - k_-^{(i)} - k^{(e)}) + 2k_{\mathrm{so}}(e^{2k^{(n)}L_n}k^{(e)} + k_-^{(i)} - k^{(n)})\cos(2k_{\mathrm{so}}L_n) - e^{2k^{(n)}L_n}4k_{\mathrm{so}}^2\sin(2k_{\mathrm{so}}L_n)], \tag{B1}$

$b_2 = -e^{-k^{(n)}L_n}[-2e^{k^{(n)}L_n}k_{\mathrm{so}}k^{(e)} + 2k_{\mathrm{so}}(k_-^{(i)} - k^{(n)})\cos(2k_{\mathrm{so}}L_n) - 4k_{\mathrm{so}}^2 e^{2k^{(n)}L_n}\sin(2k_{\mathrm{so}}L_n)],$

$b_3 = e^{-k^{(n)}L_n}\{e^{k^{(n)}L_n}k^{(e)}[k^{(e)} - k_-^{(i)}] - 4k_{\mathrm{so}}^2 e^{2k^{(n)}L_n}\cos(2k_{\mathrm{so}}L_n) + 2k_{\mathrm{so}}(k^{(n)} - k_-^{(i)})\sin(2k_{\mathrm{so}}L_n)\},$

$b_6 = -2k_{\mathrm{so}}(k^{(n)} - k_-^{(i)}) - e^{k^{(n)}L_n}k^{(e)}[2k_{\mathrm{so}}\cos(2k_{\mathrm{so}}L_n) + (k^{(e)} - k_-^{(i)})\sin(2k_{\mathrm{so}}L_n)], \quad b_7 = 4k_{\mathrm{so}}^2 e^{k^{(n)}L_n}.$

[1] E. Majorana, Nuovo Cimento **14**, 171 (1937).

[2] A. Y. Kitaev, Phys. Usp. **44**, 131 (2001).

[3] L. Fu and C. L. Kane, Phys. Rev. Lett. **100**, 096407 (2008).

[4] Y. Tanaka, T. Yokoyama, and N. Nagaosa, Phys. Rev. Lett. **103**, 107002 (2009).

[5] M. Sato and S. Fujimoto, Phys. Rev. B **79**, 094504 (2009).

[6] A. R. Akhmerov, J. Nilsson, and C. W. J. Beenakker, Phys. Rev. Lett. **102**, 216404 (2009).

[7] R. M. Lutchyn, J. D. Sau, and S. Das Sarma, Phys. Rev. Lett. **105**, 077001 (2010).

[8] Y. Oreg, G. Refael, and F. von Oppen, Phys. Rev. Lett. **105**, 177002 (2010).

[9] J. Alicea, Phys. Rev. B **81**, 125318 (2010).

[10] K. Flensberg, Phys. Rev. B **82**, 180516 (2010).

[11] M. Duckheim and P. W. Brouwer, Phys. Rev. B **83**, 054513 (2011).

[12] A. C. Potter and P. A. Lee, Phys. Rev. B **83**, 094525 (2011).

[13] X. L. Qi and S. C. Zhang, Rev. Mod. Phys. **83**, 1057 (2011).

[14] E. M. Stoudenmire, J. Alicea, O. A. Starykh, and M. P. A. Fisher, Phys. Rev. B **84**, 014503 (2011).

[15] S. Gangadharaiah, B. Braunecker, P. Simon, and D. Loss, Phys. Rev. Lett. **107**, 036801 (2011).

[16] R. M. Lutchyn and M. P. A. Fisher, Phys. Rev. B **84**, 214528 (2011).

[17] J. Klinovaja, S. Gangadharaiah, and D. Loss, Phys. Rev. Lett. **108**, 196804 (2012).

[18] J. S. Lim, L. Serra, R. Lopez, and R. Aguado, arXiv:1202.5057.

[19] For a recent comprehensive review, see J. Alicea, Rep. Prog. Phys. **75**, 076501 (2012).

[20] A. Kitaev, Ann. Phys. **303**, 2 (2003).

[21] M. H. Freedman, A. Kitaev, M. J. Larsen, and Z. Wang, Bull. Am. Math. Soc. **40**, 31 (2003).

[22] S. Bravyi and A. Kitaev, Phys. Rev. A **71**, 022316 (2005).

[23] S. Bravyi, Phys. Rev. A **73**, 042313 (2006).

[24] C. Nayak, S. H. Simon, A. Stern, M. Freedman, and S. Das Sarma, Rev. Mod. Phys. **80**, 1083 (2008).

[25] P. Bonderson, M. Freedman, and C. Nayak, Phys. Rev. Lett. **101**, 010501 (2008).

[26] J. Alicea, Y. Oreg, G. Refael, F. von Oppen, and M. P. A. Fisher, Nat. Phys. **7**, 412 (2011).

[27] N. Read and D. Green, Phys. Rev. B **61**, 10267 (2000).

[28] C. Nayak, S. H. Simon, A. Stern, M. Freedman, and S. Das Sarma, Rev. Mod. Phys. **80**, 1083 (2008).

[29] S. Sasaki, M. Kriener, K. Segawa, K. Yada, Y. Tanaka, M. Sato, and Y. Ando, Phys. Rev. Lett. **107**, 217001 (2011).

[30] J. R. Williams, A. J. Bestwick, P. Gallagher, S. S. Hong, Y. Cui, A. S. Bleich, J. G. Analytis, I. R. Fisher, and D. Goldhaber-Gordon, arXiv:1202.2323.

[31] V. Mourik, K. Zuo, S. M. Frolov, S. R. Plissard, E. P. A. M. Bakkers, and L. P. Kouwenhoven, Science **336**, 1003 (2012).

[32] M. T. Deng, C. L. Yu, G. Y. Huang, M. Larsson, P. Caroff, and H. Q. Xu, arXiv:1204.4130.

[33] L. P. Rokhinson, X. Liu, and J. K. Furdyna, arXiv:1204.4212.

[34] H.-J. Kwon, K. Sengupta, and V. M. Yakovenko, Eur. Phys. J. B **37**, 349 (2004); Low Temp. Phys. **30**, 613 (2004).

[35] D. Sticlet, C. Bena, and P. Simon, Phys. Rev. Lett. **108**, 096802 (2012).

[36] J. D. Sau, C. H. Lin, H.-Y. Hui, and S. Das Sarma, Phys. Rev. Lett. **108**, 067001 (2012).

[37] M. Cheng and R. M. Lutchyn, arXiv:1201.1918.

[38] D. Chevallier, D. Sticlet, P. Simon, and C. Bena, Phys. Rev. B **85**, 235307 (2012).

[39] B. Braunecker, G. I. Japaridze, J. Klinovaja, and D. Loss, Phys. Rev. B **82**, 045127 (2010).

[40] L. D. Landau and E. M. Lifshitz, *Quantum Mechanics (Non-Relativistic Theory)* (Pergamon, New York, 1977), Vol. 3, p. 60; S. De Vincenzo, Braz. J. Phys. **38**, 355 (2008).

[41] We note that $\mathcal{H}^{(e)}$ given in Eq. (28) is invariant under the (pseudo)time-reversal operation $\mathcal{T}$, defined (Ref. 42) by $U_T^\dagger (\mathcal{H}^{(e)})^* U_T = +\mathcal{H}^{(e)}$. Indeed, choosing $U_T = -i\tau_2 \otimes \eta_0$, we see that the former relation is satisfied, and similarly for the particle-hole symmetry $\mathcal{C}$, defined (Ref. 42) by $U_C^\dagger (\mathcal{H}^{(e)})^* U_C = -\mathcal{H}^{(e)}$, which is satisfied for $U_C = \tau_0 \otimes \eta_1$. Thus since $\mathcal{T}^2 = -1$ and $\mathcal{C}^2 = 1$, $\mathcal{H}^{(e)}$ belongs to the topological class DIII (Ref. 42). In the right/left basis $\phi^{(e)} = (R, L, R^\dagger, L^\dagger)$ the MF wave function $\Phi_M(x)$ that vanishes at the boundary [see Eqs. (34), (29)] becomes $\varphi_M = \varphi_1^{(e)} - \varphi_2^{(e)}$. Its degenerate time-reversed partner, $\mathcal{T}\varphi_M = \varphi_1^{(e)} + \varphi_2^{(e)}$, also solves the Schrödinger equation but does not satisfy the boundary condition and therefore is not a solution. In other words, $\mathcal{T}$ invariance alone is only a *necessary* condition for degeneracy: the latter can be removed by boundary conditions. For an alternative classification of $\mathcal{H}^{(e)}$, see Ref. 43.

[42] S. Ryu, A. P. Schnyder, A. Furusaki, and A. W. W. Ludwig, New J. Phys. **12**, 065010 (2010).

[43] S. Tewari and J. D. Sau, arXiv:1111.6592.

[44] A. F. Andreev, Sov. Phys. JETP **19**, 1228 (1964).

[45] R. A. Riedel and P. F. Bagwell, Phys. Rev. B **48**, 15198 (1993).

[46] We note that we search for solutions of the original Hamiltonian with quadratic dispersion and thus the wave functions and their derivatives have to be continuous everywhere.

[47] D. L. Maslov, M. Stone, P. M. Goldbart, and D. Loss, Phys. Rev. B **53**, 1548 (1996).